Draft version May 14, 2021
Typeset using LATEX twocolumn style in AASTeX631

Speckle Interferometry at SOAR in 2020

Andrei Tokovinin,[1] Brian D. Mason,[2] Rene A. Mendez,[3] Edgardo Costa,[3] Andrew W. Mann,[4] and Todd J. Henry[5]

[1]*Cerro Tololo Inter-American Observatory — NFSs NOIRLab Casilla 603, La Serena, Chile*
[2]*U.S. Naval Observatory, 3450 Massachusetts Ave., Washington, DC, USA*
[3]*Universidad de Chile, Casilla 36-D, Santiago, Chile*
[4]*Department of Physics and Astronomy, University of North Carolina at Chapel Hill, Chapel Hill, NC 27599-3255, USA*
[5]*RECONS Institute, Chambersburg, PA 17201, USA*

ABSTRACT

The results of speckle interferometric observations at the 4.1 m Southern Astrophysical Research Telescope (SOAR) in 2020, as well as earlier unpublished data, are given, totaling 1735 measurements of 1288 resolved pairs and non-resolutions of 1177 targets. We resolved for the first time 59 new pairs or subsystems in known binaries, mostly among nearby dwarf stars. This work continues our long-term speckle program. Its main goal is to monitor orbital motion of close binaries, including members of high-order hierarchies and Hipparcos pairs in the solar neighborhood. We also report observations of 892 members of young moving groups and associations, where we resolved 103 new pairs.

Keywords: binaries:visual

1. INTRODUCTION

This paper continues the series of double-star measurements made at the 4.1 m Southern Astrophysical Research Telescope (SOAR) with the speckle camera, HRCam. Previous results are published by Tokovinin, Mason, & Hartkopf (2010a, hereafter TMH10) and in (Tokovinin et al. 2010b; Hartkopf et al. 2012; Tokovinin 2012; Tokovinin et al. 2014, 2015, 2016, 2018a, 2019, 2020). Observations were made during 2020, but this work also includes earlier unpublished observations.

The structure and content of this paper are similar to other paper of this series. Section 2 reviews all speckle programs that contributed to this paper, the observing procedure, and the data reduction. The results are presented in Section 3 in the form of electronic tables archived by the journal. We also discuss new resolutions and new orbits resulting from this data set. A short summary in Section 4 closes the paper.

andrei.tokovinin@noirlab.edu
brian.d.mason.civ@mail.mil
rmendez@uchile.cl

2. OBSERVATIONS

2.1. *Observing programs*

As in previous years, HRCam (see Sect. 2.2) was used during 2020 to execute several observing programs, some with common targets. Table 1 gives an overview of these programs and indicates which observations are published in the present paper. The numbers of observations are approximate. Overall, 2348 observations were made during 2020. Here is a brief description of these programs.

Orbits of resolved binaries. New measurements contribute to the steady improvement of the quantity and quality of orbits in the Sixth Catalog of Visual Binary Star Orbits (Hartkopf, Mason & Worley 2001). See Mendez et al. (2021) as an example of this work.

Hierarchical systems of stars are of special interest because their architecture is relevant to star formation, while dynamical evolution of these hierarchies increases chances of stellar interactions and mergers (Toonen et al. 2020). We followed orbital motions of several triple systems and used these data for orbit determinations (Tokovinin & Latham 2020; Tokovinin 2020, 2021a). Some observations made in 2020 are published in the above papers. They are duplicated here

Table 1. Observing programs

Program	PI	N	Publ.[a]
Orbits	Mason, Tokovinin	562	Yes
Hierarchical systems	Tokovinin	82	Yes
Hipparcos binaries	Mendez, Horch	267	Yes
Neglected binaries	R. Gould, Tokovinin	152	Yes
Nearby K dwarfs	T. Henry	228	Yes
Nearby M dwarfs	E. Vrijmoet	354	No
TESS follow-up	C. Ziegler	355	No
Young moving groups	A. Mann	985	Yes
Stars with RV trends	B. Pantoja	195	Yes

[a] This columns indicates whether the results are published here (Yes) or deferred to future papers (No).

to provide a complete and homogeneous record of the SOAR speckle data.

Hipparcos binaries within 200 pc are monitored to measure masses of stars and to test stellar models, as outlined by, e.g., Horch et al. (2015, 2017, 2019). The southern part of this sample is addressed at SOAR (Mendez et al. 2017). This program overlaps with the general work on visual orbits.

Neglected close binaries from the Washington Double Star Catalog, WDS (Mason et al. 2001), were observed as a 'filler' at low priority. In some cases, we resolved new inner subsystems, thus converting classical visual pairs into hierarchical triples. Some WDS pairs are moving fast near periastron, allowing calculation of their first orbits after several observations at SOAR.

Nearby K and M dwarfs were observed since 2018 on the initiative of T. Henry and E. Vrijmoet. The goal is to assemble statistical data on orbital elements, focusing on short periods. The sample includes known and suspected binaries detected by astrometric monitoring, Gaia, etc. Data on M dwarfs are being published by Vrijmoet et al. (2021, in preparation), while observations of K dwarfs are reported here.

TESS follow-up received a substantial time allocation in 2020, continuing the program of 2018–2019. Its first results are published by Ziegler et al. (2020), the paper with additional data is submitted (Ziegler et al. 2021). All speckle observations of TESS targets of interest are promptly posted on the EXOFOP web site. These data are used in the growing number of papers on TESS exoplanets, mostly as limits on potential companions to exohosts.

Young moving groups and associations were selected as part of a program aimed at characterizing planets and young stellar associations with TESS (the THYME survey, Newton et al. 2019). These sources were selected from because they have been observed by TESS and are likely to be young or members of nearby stellar associations reported in the literature. The majority of stars (549) were drawn from the BANYAN survey of young moving groups within 150 pc (Gagné et al. 2018), as well as 82 members of the ScorpiusCentaurus (Sco-Cen) OB association (Sco-Cen) from Rizzuto et al. (2015) excluding those already surveyed by Tokovinin & Briceño (2020) and 261 suspected pre-main-sequence stars within 500 pc from Zari et al. (2018). For both BANYAN and Sco-Cen members, membership for targets were determined primarily using Bayesian membership probabilities based on kinematics of each star and the association using Gaia DR2 astrometry. Sources from Zari et al. (2018) were selected based on their elevated position relative to the main sequence on a color-magnitude diagram. Because all target selection relied on Gaia DR2, any systematics present in the Gaia catalog (e.g., missing binaries) will be present in the targets surveyed here. The names of these objects in the data tables begin by 'T' followed by their number in the TESS input catalog (TIC, Stassun et al. 2019).

Stars with radial velocity trends were monitored since 2016 on request from B. Pantoja, with the aim to resolve potential companions causing these trends (e.g. Pantoja et al. 2018). Five new pairs and one triple (GJ 3260) were resolved at SOAR and measured during five years.

If observations of a given star were requested by several programs, they are published here even when the other program still continues. We also publish here the measurements of previously known pairs resolved during surveys, for example in the TESS follow-up.

2.2. *Instrument and Observing Procedure*

The observations reported here were obtained with the *high-resolution camera* (HRCam) – a fast imager designed to work at the 4.1 m SOAR telescope (Tokovinin 2018). The instrument and observing procedure are described in the previous papers of these series (e.g. Tokovinin et al. 2020), so only the basic facts are reminded here. We used mostly the near-infrared I filter (824/170 nm) and the Strömgren y filter (543/22 nm), with a few observations made in the B, V, and R filters; the transmission curves of HRCam filters are given in the instrument manual In the standard observing mode, two series of 400 200×200 pixel images (image cubes) are recorded. The pixel scale is $0\farcs01575$, hence the field of view is $3\farcs15$; the exposure time is normally 24 ms. For survey programs such as TESS follow-up, we use the I filter and a 2×2 binning, doubling the field. Pairs wider than ∼1.″4 are observed with a 400×400 pixel field, and the widest pairs are sometimes recorded with the full field of 1024 pixels (16″) and a 2×2 binning.

The speckle power spectra are calculated and displayed immediately after the acquisition for quick evaluation of the results. Observations of close pairs are accompanied by observations of single (reference) stars to account for such instrumental effects as telescope vibration or aberrations. Bright stars can be resolved and measured below the formal diffraction limit by fitting a model to the power spectrum and using the reference. The resolution and contrast limits of HRCam are further discussed in TMH10 and in the previous papers of this series.

A custom software helps to optimize observations by selecting targets, pointing the telescope, and logging. Typically, about 300 targets are covered on a clear night. The observing programs are executed in an optimized way, depending on the target visibility, atmospheric conditions, and priorities, while minimizing the telescope slews. Reference stars and calibrator binaries are observed alongside the main targets as needed.

During 2020, the SOAR telescope was closed from March 18 to October 7 due to COVID-19 pandemic. The number of observations obtained in 2020, 2348, is less than in 2018 and 2019. The sporadic telescope vibration that affected HRCam observations previously (see § 3.5 in Tokovinin 2018) was much less frequent in 2020.

2.3. *Data Processing and Calibration*

The data processing is described in TMH10 and Tokovinin (2018). We use the standard speckle interferometry technique based on the calculation of the power spectrum and the speckle auto-correlation function (ACF). Companions are detected as secondary peaks in the ACF and/or as fringes in the power spectrum. Parameters of the binary and triple stars (separation ρ, position angle θ, and magnitude difference Δm) are determined by modeling (fitting) the observed power spectrum. The true quadrant is found from the shift-and-add (SAA) images whenever possible because the standard speckle interferometry determines position angles modulo 180°.

The pixel scale and angular offset are inferred from observations of several relatively wide (from 0.″5 to 3″) calibration binaries. Their motion is accurately modeled based on previous observations at SOAR. The models are adjusted iteratively (the latest adjustment in 2019 November). Measurements of those wide calibrators by Gaia (Gaia collaboration 2018) show very small systematic errors of these models (Tokovinin et al. 2019). Typical rms deviations of the observations of calibrators from their models are 0.°2 in angle and 1 to 3 mas in separation. The astrometric accuracy strongly depends on the target characteristics (larger errors at large Δm and for faint pairs), as well as on the seeing and telescope vibration. The contrast limit for companion detection also depends on the conditions, so that difficult pairs can be resolved in one observing run and unresolved in another run.

Table 2. Measurements of double stars at SOAR

Col.	Label	Format	Description, units
1	WDS	A10	WDS code (J2000)
2	Discov.	A16	Discoverer code
3	Other	A12	Alternative name
4	RA	F8.4	R.A. J2000 (deg)
5	Dec	F8.4	Declination J2000 (deg)
6	Epoch	F9.4	Julian year (yr)
7	Filt.	A2	Filter
8	N	I2	Number of averaged cubes
9	θ	F8.1	Position angle (deg)
10	$\rho\sigma_\theta$	F5.1	Tangential error (mas)
11	ρ	F8.4	Separation (arcsec)
12	σ_ρ	F5.1	Radial error (mas)
13	Δm	F7.1	Magnitude difference (mag)
14	Flag	A1	Flag of magnitude difference[a]
15	$(O-C)_\theta$	F8.1	Residual in angle (deg)
16	$(O-C)_\rho$	F8.3	Residual in separation (arcsec)
17	Ref.	A8	Orbit reference[b]

[a] Flags: q – the quadrant is determined; * – Δm and quadrant from average image; : – noisy data or tentative measures.

[b] References are provided at https://www.astro.gsu.edu/wds/orb6/wdsref.txt

3. RESULTS

3.1. *Data Tables*

The results (measures of resolved pairs and non-resolutions) are presented in exactly the same format as in Tokovinin et al. (2020). The long tables are published electronically; here we describe their content.

Table 2 lists 1735 measures of 1288 resolved pairs and subsystems, including new discoveries. The pairs are identified by their WDS-style codes based on the J2000 coordinates and discoverer designations adopted in the WDS catalog (Mason et al. 2001), as well as by alternative names in column (3), mostly from the Hipparcos catalog. Equatorial coordinates for the epoch J2000 in degrees are given in columns (4) and (5) to facilitate matching with other catalogs and databases. In the case of resolved multiple systems, the position measurements and their errors (columns 9–12) and magnitude differences (column 13) refer to the individual pairings

Table 3. Unresolved stars

Col.	Label	Format	Description, units
1	WDS	A10	WDS code (J2000)
2	Discov.	A16	Discoverer code
3	Other	A12	Alternative name
4	RA	F8.4	R.A. J2000 (deg)
5	Dec	F8.4	Declination J2000 (deg)
6	Epoch	F9.4	Julian year (yr)
7	Filt.	A2	Filter
8	N	I2	Number of averaged cubes
9	$\rho_{\rm min}$	F7.3	Angular resolution (arcsec)
10	$\Delta m(0.15)$	F7.2	Max. Δm at $0.''15$ (mag)
11	$\Delta m(1)$	F7.2	Max. Δm at $1''$(mag)
12	Flag	A1	: marks noisy data

between components, not to their photo-centers. As in the previous papers of this series, we list the internal errors derived from the power spectrum model and from the difference between the measures obtained from two data cubes. The real errors are usually larger, especially for difficult pairs with substantial Δm and/or with small separations. Residuals from orbits and from the models of calibrators, typically between 1 and 5 mas rms, characterize the external errors of the HRcam astrometry.

The flags in column (14) indicate the cases where the true quadrant is determined (otherwise the position angle is measured modulo 180°), when the relative photometry of wide pairs is derived from the long-exposure images (this reduces the bias caused by speckle anisoplanatism), and when the data are noisy or the resolutions are tentative (see TMH10). For binary stars with known orbits, the residuals to the latest orbit and its reference are provided in columns (15)–(17).

Non-resolutions are reported in Table 3. Its first columns (1) to (8) have the same meaning and format as in Table 2. Column (9) gives the minimum resolvable separation when pairs with $\Delta m < 1$ mag are detectable. It is computed from the maximum spatial frequency of the useful signal in the power spectrum and is normally close to the formal diffraction limit λ/D. The following columns (10) and (11) provide the indicative dynamic range, i.e. the maximum magnitude difference at separations of $0.''15$ and $1''$, respectively, at 5σ detection level. The last column (12) marks noisy data by the flag ":".

Table 2 contains 162 pairs resolved for the first time; some of those were confirmed in subsequent observing runs. In the following sub-sections we discuss the new pairs.

3.2. *Young Moving Groups and Associations*

Table 4. New YMG Pairs

WDS	TIC	ρ (arcsec)	ΔI (mag)	N[a]
00376−2709	246895416	0.14	2.5	4
02002−8025	273789976	0.03	0.0	3
02109−4604	7242537	0.21	2.9	2
02489−3404	122671519	0.05	0.0	2
02568−6343	220556639	0.07	0.0	3
03165−3541	176832633	0.19	4.4	3
03259−3556	142874733	0.06	2.3	3
04001−2902	44670258	0.07	2.4	1?
04084−2745	44793998	0.37	1.5	2
04316−3043	170699229	0.44	1.6	1
04536−2836	671393	0.13	0.0	2
05085−2102	146539195	0.05	0.6	3
05287−3327	24448282	0.14	1.2	2
05371−3932	144499196	0.16	1.3	2
05412−4118	21438160	0.07	0.0	3
05425−1535	46739994	1.15	0.7	1
05471−3211	100608178	0.27	1.0	1
05473−5450	350563576	0.84	5.0	1
05504−2915	32930236	0.85	3.6	1
05597−6209	149935360	1.15	4.0	1
06086−3403	201391310	0.57	3.1	1
06086−5704	260127241	0.12	0.0	1
06220−7932	270424741	0.06	0.0	1
06462−8359	397231463	1.45	5.7	1
07019−3922	157212164	1.83	4.1	1
07147−4010	22766740	0.16	0.1	2
07310−8419	405077613	0.61	3.8	1
07336−4019	173957127	1.70	−0.15	1*
07336−4019	173957127	0.12	0.6	1*
07406−6704	300741570	2.27	3.4	1
07418−4630	123642034	1.49	1.2	1
07437−6107	281582156	0.18	3.4	2
07571−2227	142844055	1.16	1.1	1
08262−3902	183974196	0.24	0.1	1
09095−5538	385012516	0.05	0.1	4
10054−7137	372515598	0.10	0.0	2
10056−5731	462492721	3.85	4.0	1
10074−4622	311258541	0.18	0.1	2
10207−6311	378126824	0.32	1.4	2
10330−6144	460604193	0.52	4.5	1
11081−6342	466799461	2.37	5.4	1
11098−3828	151738485	0.05	1.1	1?
11099−3739	151762498	0.06	0.6	1
11262−5823	451452509	0.11	1.6	1
11545−5325	400913139	0.03	0.7	1?
12172−1033	203233128	0.12	0.4	1
12269−3316	130722957	0.67	0.1	1
12328−7654	360339486	0.17	1.0	2
12559−7417	361525866	1.10	0.7	2

Table 4 *continued*

Table 4 *(continued)*

WDS	TIC	ρ (arcsec)	ΔI (mag)	N[a]
12577−6652	335287811	0.13	0.3	3
13090−5720	253501247	4.10	0.9	1
13123−5441	406376573	1.00	0.9	1
13137−5807	406694754	0.68	1.0	2
13260−5112	438733975	0.11	1.1	3
13271−4856	438790187	0.95	2.5	2
13275−4719	438627800	2.82	4.4	1
13341−5624	457308993	1.12	0.1	1*
13341−5624	457308993	0.09	0.0	1*
13413−4537	243415454	3.59	1.6	1
13415−4431	243425206	2.47	0.0	1*
13415−4431	243425206	0.66	0.1	1*
13453−4102	166302995	0.31	3.1	1
13485−6727	429383724	0.71	2.8	1
13491−4413	243621789	2.92	4.9	1
13523−3826	166624597	0.13	1.3	1
13538−5502	208387087	3.17	0.5	1
13579−4432	359830202	0.17	2.2	1
14028−1850	6119516	1.80	0.8	1
14161−4031	179793360	0.17	2.2	2
14169−3648	179819049	0.08	0.0	1
14171−4038	179829109	0.96	3.2	1
14241−3923	167542104	1.50	1.6	1
14381−4322	128453434	1.11	1.6	1
14463−5056	250091359	0.63	2.2	1
14535−3903	160451137	1.04	2.6	1
14541−3606	160574439	0.08	0.8	1
14544−3718	160576551	3.26	0.6	1
14592−4012	121196256	2.50	0.9	1
15180−3335	272248916	0.08	0.0	2
15206−3132	460325085	1.22	2.1	1
15230−3052	54077774	2.17	0.6	1*
15230−3052	54077774	0.36	1.1	1*
15233−3127	54077130	3.35	0.2	1
15280−3208	54512674	2.22	2.4	1
15299−3136	54667962	1.73	2.4	1
15312−3505	54802536	0.08	0.7	2
15476−3127	442571495	0.07	0.0	1
16186−3839	318141352	1.66	5.2	1
16210−0617	135890809	0.05	0.2	1
16223−3843	4061225	0.81	1.9	1
16338−5119	22836043	1.81	3.1	1*
16338−5119	22836043	0.13	1.1	1*
16345−1106	152667565	1.95	0.7	1
16361−1324	414338264	1.21	5.6	1
16498−1239	398869084	0.60	3.8	1
16502−1108	181292505	0.76	2.4	1
17076−0515	142638811	0.23	2.5	1
17123−1131	146003265	0.09	0.0	1
17142−0038	176322832	0.48	2.9	1
17185−7858	384747990	0.12	0.4	1
17563−5833	337276808	1.85	1.3	1

Table 4 *continued*

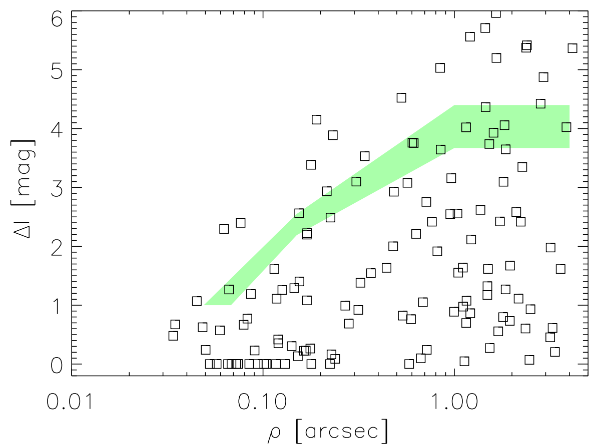

Figure 1. Resolved pairs in the YMG sample: ΔI vs. separation. The shaded green area depicts the lower and upper quartiles of the detection limits.

Table 4 *(continued)*

WDS	TIC	ρ (arcsec)	ΔI (mag)	N[a]
20108−3845	269768590	1.37	2.6	2
20146−5431	201751726	0.58	0.0	1
21123−8129	403995704	0.10	0.0	1
21210−5229	79403459	0.09	0.2	4
21215−6655	419610508	0.06	1.3	1
21589−4706	389726031	0.15	0.0	3

[a] The question mark indicates unreliable resolutions, asterisks distinguish triple stars.

The TESS follow-up program started in 2018. It was complemented by a sample of the members of young moving groups and associations (YMGs) based on the TESS input catalog, TIC (Stassun et al. 2019) and Gaia astrometry. These objects are identified here by TIC numbers preceded by the letter ‘T’. Overall, 892 objects from this program were observed at least once. The largest number of observations (608) were secured in 2019, and only 32 in 2020; the total number of observations is 985 (some newly resolved pairs were re-visited).

Figure 1 plots the magnitude difference ΔI vs. separation ρ for resolved pairs of the YMG sample. One notes the paucity of pairs with separations from $0\farcs2$ to $0\farcs7$ and a small ΔI. Such near-equal pairs do not have astrometry in Gaia and, for this reason, were not included in the sample which, therefore, is biased against such binaries.

There are 129 resolved pairs among 892 YMG objects, so the observed raw multiplicity rate is 14.5 per cent. Most of these pairs (103) are new discoveries. Statistical analysis of the multiplicity is outside the scope of

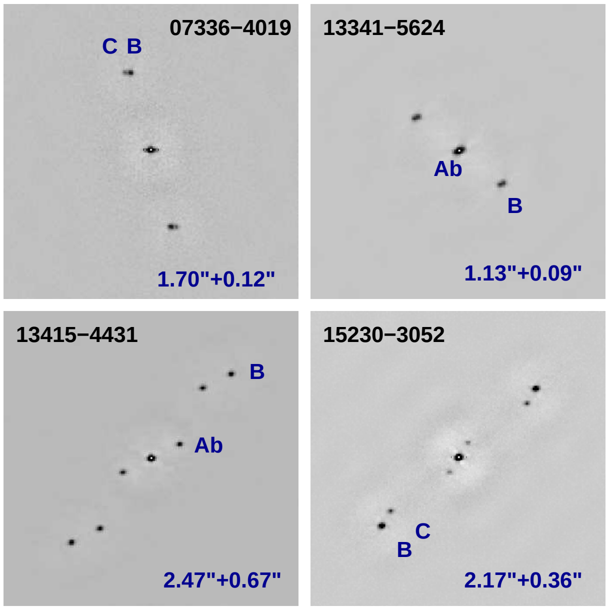

Figure 2. Four new triples in the YMG sample. The panels show speckle ACFs (in negative rendering) in the full 3.″15 field. The letters mark secondary peaks corresponding to the companions (as opposed to the mirror peaks) inferred from the SAA images. The separations of the outer and inner pairs in arcseconds are given in the lower-right corner.

this paper, which only reports the observations. Some companions, especially those with large ρ and ΔI, can be unrelated stars (optical pairs). All newly resolved YMG pairs are listed in Table 4. They are identified by the WDS-style code and the TIC numbers. The following columns contain the separation ρ, the magnitude difference ΔI, and the number of visits N where the pair was resolved. Mostly, we re-visited close pairs and found that some of them show rapid orbital motion on the time span of 1–3 yrs. They are promising candidates for future orbit determinations and measurements of masses. Three new close pairs were not resolved in subsequent visits either because they moved under the resolution limit or because the first resolutions were unreliable. These stars can be in fact single; they are distinguished by question marks in the last column, and further observations are needed to confirm these pairs.

The resolution and contrast limits depend on the seeing and target magnitude. One might think that brighter targets have a larger chance of binary detection. However, the median TESS magnitudes T of the resolved and unresolved targets are 11.4 and 11.5 mag, respectively, and their distributions look alike. Therefore, the magnitude bias is small, if any. The total range of magnitudes in this sample is from $T = 6$ to $T = 13$ mag.

Five YMG targets turned out to be resolved triple stars. They have two entries in Table 4 (one per subsystem), marked by asterisks in the last column. Figure 2 illustrates the ACFs of four new young triples out of five.

3.3. *Other New Pairs*

Table 5 highlights 59 pairs resolved in 2020 or resolved earlier but not yet published. All measurements of these pairs are found in Table 2. Table 5 is similar to Table 4, but it contains an additional column specifying the program. The largest number of new pairs, 36, comes from the survey of K-type dwarfs. Most of these were observed more than once, and some (the closest) are in rapid orbital motion. The combined spectro-interferometric orbit of one such pair, HIP 57058, is determined (Figure 4). Five pairs are serendipitous resolutions of reference stars (three of those predate 2020 but were not reported previously), two are new close subsystems in classical visual binaries (WDS program), and three are subsystems in multiple stars (MSC). Most new pairs are real physical binaries, and a few appear to be optical (chance projections).

3.4. *New and updated orbits*

New positional measurements furnished by the SOAR speckle program provide material for calculation of new visual orbits and improvement of the known ones. The previous paper of this series (Tokovinin et al. 2020) gave a long list of new orbits. Here we only give references on the latest orbits resulting from this program (Mendez et al. 2021; Tokovinin & Latham 2020; Tokovinin 2021a,b) and provide examples in Figures 3 and 4. The orbital elements are published, so there is no need to repeat them here. We comment on each pair below.

00219−2300 (ADS 302, HIP 1732) is a triple system at 60 pc from the Sun. The pair BC is located at 6.″1 from the main star A and composed of similar K-type dwarfs. Five micrometric measures made since its discovery by S. Rossiter in 1949 were insufficient for orbit calculation, and we see why: the orbit is oriented edge-on and has a large eccentricity $e = 0.83$. The pair was monitored at SOAR since 2008; it closed down and opened again this year after passing through the periastron. The mass sum is 1.5 $\mathcal{M}_\odot$.

01077−1557 (HIP 5295) is a pair of solar-type dwarfs discovered by Hipparcos. Its first 15.5 yr orbit is based exclusively on the 10 SOAR measures because the Hip-

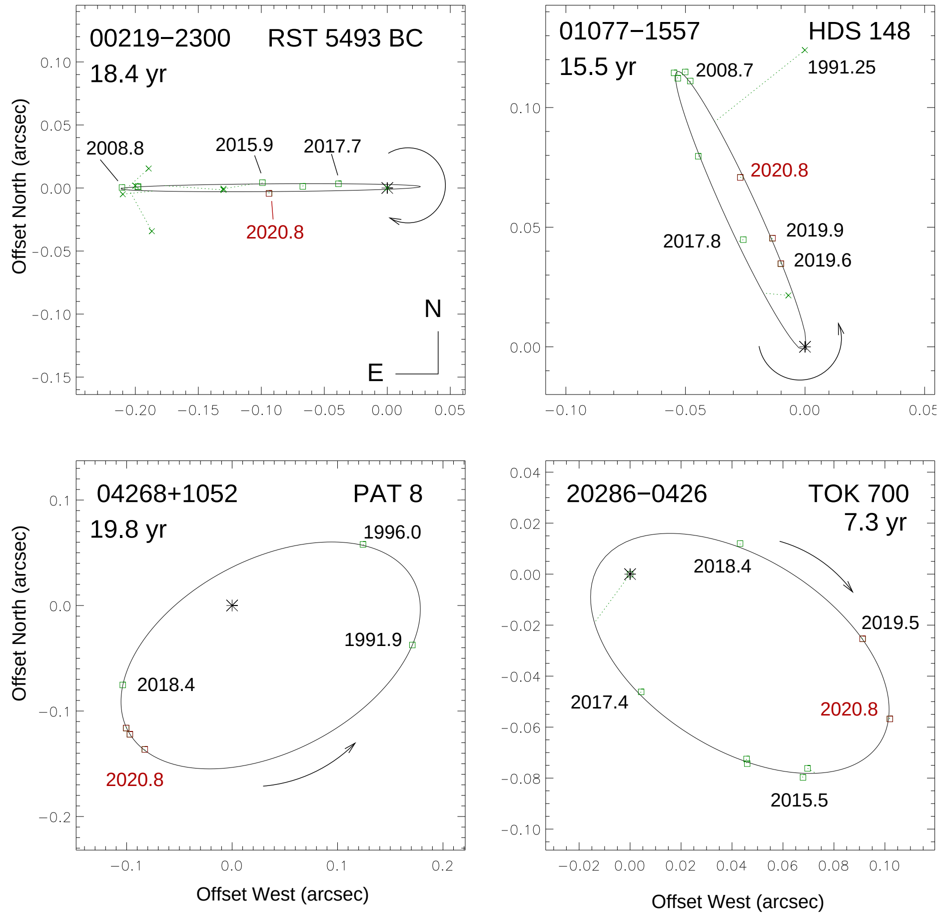

Figure 3. Four first-time orbits computed using the SOAR observations in 2020. Accurate speckle measurement are plotted as squares (in red after 2019.0), visual micrometer measurements as crosses. The axis scale is in arcseconds.

parcos measurement appears to be misleadingly inaccurate. We observed the pair in 2008 near maximum separation; it passed through the periastron of eccentric ($e = 0.98$) orbit in 2019.1 (an uncertain measure was attempted in 2018 below the diffraction limit) and became resolved again in 2019. Although this is a first-time orbit, its elements are quite accurate.

04268+1052 (HIP 20751) is a K0V binary dwarf in the Hyades. Only two measurements were available before 2018, when the SOAR observations started as part of the K-dwarf survey. The arc observed at SOAR is quite short, but, combined with the historic measurements, it allows the calculation of the first 20 yr orbit. The periastron in 2017.4 was, unfortunately, missed, and now the pair is on a slow segment of its orbit. The fit of the 7 orbital elements to the 6 position measurements is nearly perfect (residuals less than 1 mas).

20286–0426 (HIP 100988) is another pair of solar-type stars discovered at SOAR in 2015.5. Its monitoring to date allows calculation of the first 7.3 yr orbit, now almost completely covered.

These four pairs chosen to illustrate new orbits have something in common. They are composed of low-mass stars and their orbits have substantial eccentricities, from 0.65 to 0.98. Radial velocity (RV) monitoring near the periastron can furnish direct measurements of the mass ratios and orbital parallaxes. Such observations can be planned in the future, knowing the visual elements. One notes that the 11 yr duration of the extended Gaia mission is not long enough to derive astrometric orbits from the photo-center motion, while these pairs are too close for a direct resolution by Gaia. However, future combination of speckle orbits and Gaia astrometry will allow accurate modeling of the photo-center motion, leading to unbiased measurements of the parallaxes and, hence, masses.

Figure 4 illustrates the synergy between interferometric and spectroscopic data for the case of a nearby K4V dwarf HIP 57058 (GJ 435.1, distance 31 pc). It was previously identified as a double-lined spectroscopic binary. A preliminary spectroscopic orbit with a period of 725.9 days (2.00 yr) was published by Sperauskas et al. (2019), who also mention its first resolution at SOAR in 2018.2.

Table 5. New Double Stars

WDS	Name	ρ (arcsec)	Δm (mag)	N	Prog.[a]
00111+0513	HIP 898	0.12	2.5	2	NKD
01027−2519	HIP 4874	0.10	3.4	6	NKD
01262+1349	HIP 6705	0.79	3.6	2	NKD
01406+0846	HIP 7819	0.09	1.3	2	REF
02035−0455	HIP 9603	0.20	2.9	4	NKD
02324+0323	HIP 11815	1.50	3.1	2	NKD
03225+1744	HIP 15724	1.70	7.4	2	NKD
04007−2305	GJ 3260AB	1.35	2.6	7	Pan
04007−2305	GJ 3260BC	0.33	0.1	7	Pan
04141−3155	TIC168789840	0.42	0.3	4	TESS
04234+1546	HIP 20485	1.20	4.5	2	NKD
04279+2427	HIP 20834	0.17	2.7	4	NKD
04330−1633	HIP 21222	0.09	1.7	7	NKD
04518+1339	BU 552Ba,Bb	0.04	1.2	2	MSC
06006−5806	HIP 28464	0.44	4.5	2	REF
06215+1718	HIP 30220	0.92	3.0	3	NKD
06443−2349	TDS4085BC	0.33	0.4	1	TESS
07151+1556	HIP 35071	1.10	2.6	2	NKD
07390+1913	HIP 37246	0.44	1.4	3	NKD
07584−1501	HIP 38969	0.11	3.1	2	NKD
08155+0959	HIP 40449	0.23	0.1	3	NKD
08187−1512	HIP 40724	0.07	2.3	8	NKD
08253+0415	HIP 41277	0.35	3.7	3	NKD
08430+2408	TOK 265Aa,Ab	0.18	2.2	4	NKD
09095−0024	HIP 44953	1.38	3.7	2	NKD
09308+1815	HIP 46662	0.14	2.7	5	NKD
09361−5145	RST 415Aa,Ab	0.14	1.7	1	TESS
09380+2231	HIP 47261	1.11	3.7	2	NKD
09429−5502	RST3660Aa,Ab	0.07	1.3	3	WDS
09527−7933	KOH 86Aa,Ab	0.04	1.7	1	MSC
10041+1848	HIP 49324	0.13	0.1	6	NKD
10211−1744	HIP 50696	0.59	1.2	3	NKD
10212−5143	I 853Ba,Bb	0.09	1.0	3	WDS
10262−6318	HIP 51083	0.10	2.5	2	REF
10283−2416	HIP 51263	0.20	2.0	6	NKD
10527+0029	HIP 53175AB	1.65	3.0	4	NKD
10527+0029	HIP 53175BC	0.17	1.2	4	NKD
11100−1017	HIP 54569AB	0.37	3.1	4	NKD
11100−1017	HIP 54569Aa,Ab	0.04	0.1	4	NKD
11358+2437	HIP 56570	0.39	3.4	2	NKD
11418+0508	HIP 57058	0.06	0.0	7	NKD
11563+1102	SKF 256Aa,Ab	0.89	4.2	2	NKD
12104−4352	HD 105750	0.06	1.3	13	Pan
12356−3454	GJ 1161B	0.33	0.1	7	Pan
13344−2730	HIP 66229	0.04	1.5	3	NKD
14106−2826	HIP 69249	0.24	2.6	4	NKD
14232−6302	FIN 221Aa,Ab	0.10	2.2	1	TESS
15003+0739	HIP 73424	0.18	4.6	1?	REF
15481−5811	SKF2839Aa,Ab	0.26	1.5	5	Pan
16238−0258	HIP 80315	0.20	3.8	2	NKD
17190−4638	HD 156274B	0.04	1.9	8	Pan
17331−3035	CHM 6BC	3.09	5.0	2	NKD
18185−3441	HIP 89708	0.18	3.5	1	REF
19443−2657	HD 186265	1.06	5.0	5	Pan
20118−3825	RTW2011AB	4.23	0.1	1	NKD
22412−1625	RTW2241AB	4.48	0.1	1	NKD
22590−0432	BD−05 5901	0.42	1.2	1	MSC
23231−7747	UC 4934Aa,Ab	0.12	0.4	1	HIP
23343+0932	HIP 116334	0.37	3.7	4	NKD

[a] HIP – *Hipparcos* suspected binary; NKD – nearby K-dwarfs; MSC – multiple system; Pan – program by B. Pantoja; REF– reference star; TESS – TESS follow-up; WDS – neglected pair.

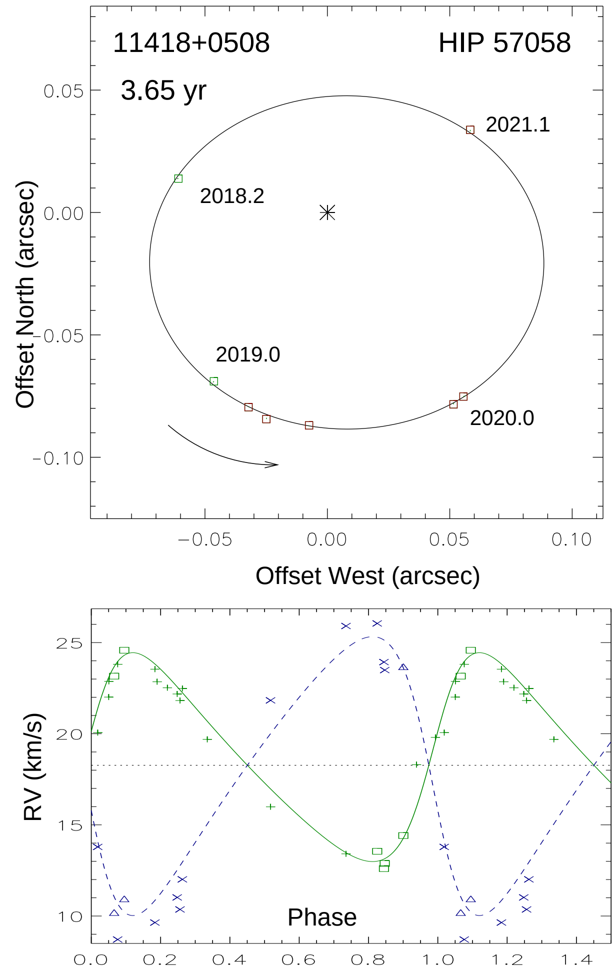

Figure 4. Orbit of HIP 57058 in the plane of the sky (top) and its RV curve (bottom).

The pair was also resolved in 2016 by T. Henry, but this measurement is not yet published. Continued monitoring at SOAR revealed that the observed motion is not compatible with the 2 yr period, and the true period is two times longer. Stars A and B are similar ($\Delta I = 0.3$ mag), and a wrong attribution of radial velocities (RVs) to a particular component was the reason for the incorrect spectroscopic orbit (which is single-lined despite the double-lined nature of the system). The new orbit with $P = 3.65$ yr presented in Figure 4 uses only RVs of both components when they were resolved spectroscopically. The RV curves look noisy, but, considering the small amplitudes (5.7 and 7.7 km s^{-1}) and the difficulty of measuring blended spectra, barely resolved only near the RV maximum, the rms residuals of 0.4 and 1.2 km s^{-1} appear quite acceptable. The residuals of the interferometric measures are small, under 1 mas. The mass sum of 1.35 $\mathcal{M}_\odot$ computed from the orbit and the

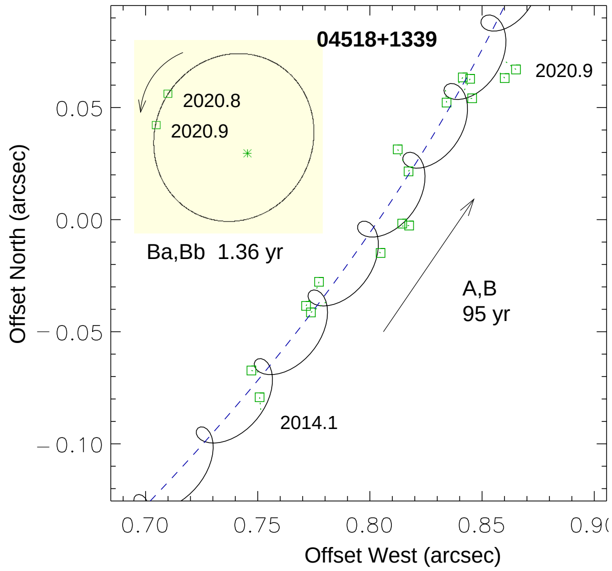

Figure 5. Wavy motion of the visual binary J04518+1339 (BU 552) caused by the subsystem Ba,Bb, and the orbit of Ba,Bb (insert) deduced from the RVs and two measures at SOAR.

Gaia parallax matches the RV amplitudes and the spectral type.

3.5. *Hierarchical systems*

Accumulation of accurate speckle measures with dense coverage made at SOAR allows the study of relative motions in hierarchical stellar systems. The latest papers in this area were already cited (Tokovinin & Latham 2020; Tokovinin 2020, 2021a). Here two additional examples are given.

J04518+1339 (HD 30869, HIP 22607) is a quadruple system belonging to the Hyades cluster. The outer visual pair BU 552 has been known since 1877, and its 95 yr orbit is very well defined by observations covering 1.5 revolutions. Components A and B are double-lined spectroscopic binaries with periods of 143.6 and 496.7 days, respectively (Tomkin et al. 2007). The estimated semimajor axis of Ba,Bb is 33 mas, favoring detection of wobble caused by this subsystem, while the astrometric orbit of Aa,Ab with an amplitude of 4.4 mas was computed by Ren & Fu (2013). From 2016 on, this binary was frequently observed at SOAR. In 2020, the slight elongation of the secondary ACF peak was noted and a triple-star model was fitted, tentatively resolving Ba,Bb on two occasions. Similar elongation can be suspected upon examination of previous observations, but it is often concealed by false elongation due to telescope vibration or charge-transfer problem; only observations of the highest quality in the filter y allow marginal resolutions of Ba,Bb at phases near its maximum separation. Figure 5 shows the two measures of Ba,Bb that fit nicely the orbit of Tomkin et al. (2007) with additional elements $a = 34$ mas, $\Omega = 326°$, and $i = 32°$. The axis and inclination match their estimates derived from the spectroscopic orbit. Moreover, the wobble in the motion of A,B with a period of 1.36 yr is rather obvious; its amplitude is 9.7 mas. Motion of the photocenter of A with a 143 day period increases the residuals.

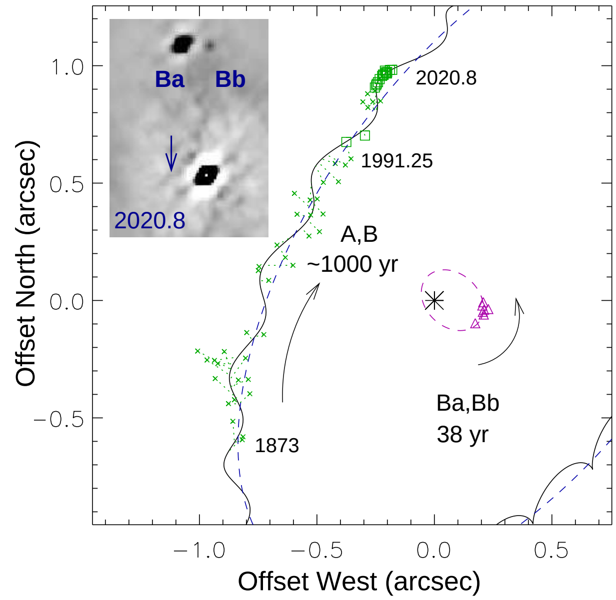

Figure 6. Orbital motion of J02460−0457. The wavy line is the motion of A,B with wobble. Squares depict accurate measures from Hipparcos and speckle, crosses are micrometer measures. The inner orbit Ba,Bb is plotted around the center on the same scale by magenta ellipse and triangles. The insert shows the speckle ACF recorded in 2020.8 where the blue arrow shows the missing ACF peak (see text).

Tomkin et al. (2007) estimate orbital inclination of Aa,Ab to be around 49°, suggesting possible coplanarity with the orbit of A,B (inclination 51°). Ren & Fu (2013) found that the nodes of A,B and Aa,Ab have similar position angles, but they give a mismatching inclination of 94.°4 for Aa,Ab. Our work establishes the orientation of the orbit of Ba,Bb: it is inclined to the orbit of A,B by 26°. These preliminary results should be refined by further observations, preferably with larger aperture (the resolution of Ba,Bb at SOAR is just marginal).

J02460−0457 (HD 17251, HIP 12912) is a triple system where the outer pair A,B (BU 83) has been known since 1873. A third faint component was discovered at SOAR in 2016 and attributed to the primary (Tokovinin et al. 2018a), based on the sign of the wobble. Continued observations show that this is not correct and the faint companion in fact belongs to the secondary star B. The situation is illustrated in Figure 6. Generally, the ACF of a triple star contains 6 secondary peaks corresponding to 6 vectors between its components. The relative intensity of the peaks is proportional to the products of the relative fluxes; the two weakest peaks that correspond to the pair of the faintest stars often are lost in the noise, as is the case here. The arrow shows the position of the missing peak corresponding to the faint companion. If it were associated with A, this missing peak would be stronger than the well-visible peak Bb. The missing peak was marginally seen in the discovery ACF, prompting the original wrong attribution of the new companion.

The rotation direction of Ba,Bb pair is opposite to A,B. Existing data were reprocessed with the assumption that the companion is associated with B, resulting in more accurate measurements of the Ba,Bb positions. The wave in the A,B motion does not depend on the choice, so the original argument associating the companion with A was not valid. If the new companion were associated with A, the wobble should produce a proper motion (PM) anomaly (difference between the Gaia short-term PM and the long-term PM of the photocenter) of about 2 mas yr^{-1}, oriented in the declination direction. The measured PM anomaly in declination is 0.15±0.14 mas yr^{-1}, compatible with zero; it proves that the subsystem is associated with component B.

The inner and outer orbits fitted to the available measures, shown in Figure 6, are still preliminary. The opposite sense of rotation excludes their coplanarity: the mutual inclination is either 130° or 95°. Unequal masses and misaligned, eccentric orbits are signs of dynamical interactions that probably defined the architecture of this triple system.

4. SUMMARY

The total number of observations made with HRCam to date is about 25,000. This paper documents the observations made in 2020, as well as earlier unpublished data. The HRCam at SOAR is used by various programs, executed in a concerted and optimized way and complemented by the uniform data reduction and calibration procedures. Focused initially on the determination of visual orbits, the programs expanded into surveys of binarity in various populations. Still, the orbits of both previously known pairs and those discovered at SOAR remain the major use of the HRCam data.

This paper presents results of the large survey of YMG population and of the K-type dwarfs in the solar neighborhood. Both programs discovered a substantial number of tight pairs with fast orbital motion. Their continued monitoring will lead to orbit calculation and measurements of masses in the near future. For example, the first orbit of the K-dwarf HIP 57058 presented above uses two years of SOAR data in combination with the longer RV coverage. Several orbits of new M-dwarf pairs with short periods will be published by E. Vrijmoet et al. (2021, in preparation).

Flexibility of the HRCam observing procedure brings unexpected benefits. When the unusual sextuple eclipsing system TIC 168789840 (J04141−3155) was discovered, it could be quickly tested at SOAR and resolved into a $0\farcs4$ pair — a key piece of information for unveiling the architecture of this unique object (Powell et al. 2021). Thus, the ongoing SOAR speckle program is a backbone for testing future discoveries in a quick and efficient way.

We thank the SOAR operators for efficient support of this program, and the SOAR director J. Elias for allocating some technical time. This work is based in part on observations carried out under CNTAC programs CN2019A-2, CN2019B-13, CN2020A-19, and CN2020B-10.

R.A.M. and E.C. acknowledge support from the FONDECYT/CONICYT grant # 1190038. T. Henry appreciates support of this work through NSF grants AST-1517413 and AST-1910130.

This work used the SIMBAD service operated by Centre des Données Stellaires (Strasbourg, France), bibliographic references from the Astrophysics Data System maintained by SAO/NASA, and the Washington Double Star Catalog maintained at USNO. This work has made use of data from the European Space Agency (ESA) mission Gaia (https://www.cosmos.esa.int/gaia) processed by the Gaia Data Processing and Analysis Consortium (DPAC, https://www.cosmos.esa.int/web/gaia/dpac/consortium). Funding for the DPAC has been provided by national institutions, in particular the institutions participating in the Gaia Multilateral Agreement.

Facilities:

Facility: SOAR.

REFERENCES

Gagné, J., Mamajek, E. E., Malo, L., et al. 2018, ApJ, 856, 23 doi: 10.3847/1538-4357/aaae09

Gaia Collaboration, Brown, A. G. A., Vallenari, A., Prusti, T., et al. 2018, A&A, 616, 1 (Vizier Catalog I/345/gaia2).

Hartkopf, W. I., Mason, B. D. & Worley, C. E. 2001, AJ, 122, 3472

Hartkopf, W. I., Tokovinin, A. & Mason, B. D. 2012, AJ, 143, 42

Horch, E. P., van Belle, G. T., Davidson, J. W., Jr., et al. 2015, AJ, 150, 151

Horch, E. P., Casetti-Dinescu, D. I., Camarata, M. A., et al. 2017, AJ, 153, 212

Horch, E. I., Tokovinin, A., Weiss, S. A., et al. 2019, AJ, 157, 56

Jones, J., White, R. J., Boyajian, T., et al. 2015, ApJ, 813, 58

Mason, B. D., Wycoff, G. L., Hartkopf, W. I., et al. 2001, AJ, 122, 3466 (WDS)

Mendez, R. A., Claveria, R. M., Orchard, M. E., & Silva, J. F. 2017, AJ, 154, 187

Mendez, R. A., Clavería, R. M., & Costa, E. 2021, AJ, 161, 155

Newton, E. R., Mann, A. W., Tofflemire, B. M., et al. 2019, ApJL, 880, L17

Pantoja, B. M., Jenkins, J. S., Girard, J. H., et al. 2018, MNRAS, 479, 4958

Powell, B. P., Kostov, V., Rappaport, S. A., et al. 2021, AJ, 161, 162

Ren, S. & Fu, Y. 2013, AJ, 145, 81

Rizzuto, A. C., Ireland, M. J., & Kraus, A. L. 2015, MNRAS, 448, 2737, doi: 10.1093/mnras/stv207

Sperauskas, J., Deveikis, V., & Tokovinin, A. 2019, A&A, 626, 31

Stassun, K. G., Oelkers, R. J., Paegert, M., et al. 2019, AL, 158, 138

Tokovinin, A. 2012, AJ, 144, 56

Tokovinin, A. 2016a, AJ, 152, 138

Tokovinin, A. 2017, AJ, 154, 110

Tokovinin, A. 2018, PASP, 130, 5002

Tokovinin, A. 2020, AstL, 46, 612

Tokovinin, A. 2021a, AJ, 161, 144

Tokovinin, A. 2021b, Inf. Circ., 203, 1

Tokovinin, A. & Briceño, C. 2020, AJ, 159, 15

Tokovinin, A. Cantarutti, R., Tighe, R., et al. 2010b, PASP, 122, 1483

Tokovinin, A. & Latham, D. W. 2020, AJ, 160, 251

Tokovinin, A., Mason, B. D., & Hartkopf, W. I. 2010a, AJ, 139, 743 (TMH10)

Tokovinin, A., Mason, B. D., & Hartkopf, W. I. 2014, AJ, 147, 123

Tokovinin, A., Mason, B. D., Hartkopf, W. I., et al. 2015, AJ, 150, 50

Tokovinin, A., Mason, B. D., Hartkopf, W. I., et al. 2016, AJ, 152, 116

Tokovinin, A., Mason, B. D., Hartkopf, W. I., et al. 2018, AJ, 155, 235

Tokovinin, A., Mason, B. D., Mendez, R. A., et al. 2019, AJ, 158, 148

Tokovinin, A., Mason, B. D., Mendez, R. A., et al. 2020, AJ, 160, 7

Tomkin, J., Griffin, R. F., & Alzner, A. 2007, Obs, 127, 87

Toonen, S., Portegies Zwart, S., Hanera, A. S., & Bandopadhyay, D. 2020, A&A, 640, 16

Zari, E., Hashemi, H., Brown, A. G. A., Jardine, K., & de Zeeuw, P. T. 2018, A&A, 620, A172

Ziegler, C., Tokovinin, A., Briceño, C., et al. 2020, AJ, 159, 19

Ziegler, C., Tokovinin, A., Latiolais, M., et al. 2021, AJ, submitted